In situ Assessment of Intraepithelial Neoplasia in Hamster Trachea Epithelium Using Angle-Resolved Low-Coherence Interferometry

Kevin J. Chalut,[1] Laura A. Kresty,[2] John W. Pyhtila,[1] Ronald Nines,[2] Maureen Baird,[2] Vernon E. Steele,[3] and Adam Wax[1]

[1]Department of Biomedical Engineering, Duke University, Durham, North Carolina; [2]The Ohio State University Comprehensive Cancer Center, Columbus, Ohio; and [3]Division of Cancer Prevention, National Cancer Institute, Bethesda, Maryland

Abstract

Optical spectroscopy was used to evaluate the transformation of nuclear morphology associated with intraepithelial neoplasia in an animal model of carcinogenesis. In this pilot study, we have assessed the capability of angle-resolved low-coherence interferometry (a/LCI) to monitor *in situ* the neoplastic progression of hamster trachea epithelial tissue. By using the depth resolution made possible by coherence gating, the a/LCI system has been adapted to the unique geometry of the hamster trachea to allow us to extract useful nuclear morphometric information from cells in the epithelial layer without the need for exogenous staining or tissue fixation. Analysis of a/LCI nuclear morphology measurements has identified two important biomarkers of neoplastic transformation in hamster trachea epithelium, the size and the refractive index of epithelial cell nuclei. By comparing the a/LCI measurements of these two biomarkers to pathologic classification, we distinguished nuclear morphology changes for normal tissue, low-grade dysplasia, and high-grade dysplasia. Given its previous usefulness for tracking neoplastic change through nuclear morphometry measurements, the a/LCI technique may prove to be a useful tool in evaluating chemopreventive agents in future studies of hamster trachea epithelium. (Cancer Epidemiol Biomarkers Prev 2007;16(2):223–7)

Introduction

Lung cancer is the most common cause of cancer mortality; the 5-year survival rate for all diagnosed lung cancers is between 10% and 15% (1). Most lung tumors are bronchogenic carcinomas, which are a malignant neoplasm of the lung arising in the epithelium of the bronchus or bronchiole (2). Squamous cell carcinoma, a particular type of bronchogenic carcinoma, is morphologically similar to methylnitrosourea (MNU)–induced tumors in the Syrian golden hamster respiratory tract. The progress of MNU-induced tumors, from normal epithelium to dysplasia, carcinoma *in situ*, and eventually infiltrating squamous cell carcinoma, is similar to the metaplastic evolution of squamous cell carcinoma in human lungs (3, 4). Because of this similarity, it is appropriate to study pulmonary carcinogenesis and the efficacy of candidate chemopreventive agents in this model. To achieve this goal, extensive studies will be done that use an optical spectroscopic technique, angle-resolved low-coherence interferometry (a/LCI), to detect neoplastic change in the respiratory tract of the Syrian golden hamster. This article presents a pilot study that tested the feasibility of using the a/LCI technique for these studies and further enhanced its ability to detect disease progression in this model.

The a/LCI technique combines the two concepts of low-coherence interferometry and light scattering spectroscopy. Low-coherence interferometry uses coherence gating to isolate singly scattered light from the epithelial layer in this study, which can yield valuable information about structural changes associated with neoplastic transformation. Without the depth resolution obtained via coherence gating, this information can be obscured by diffuse scattering from subsurface layers. Coherence gating is also used to obtain depth resolution in optical coherence tomography, a technique used to obtain tomographic images of living tissues (5, 6). The a/LCI technique further uses the principles of light scattering spectroscopy, which analyzes scattering information to determine structure. With this combination, the a/LCI technique offers the ability to obtain structural information with subwavelength precision and accuracy (7), which is beyond the capability of optical coherence tomography or other ordinary imaging techniques.

In application to probing tissues, a/LCI assesses neoplastic change in the epithelial layer of tissue through quantitative nuclear morphology measurements without the need for exogenous staining or tissue removal. Previously, the a/LCI system has been successfully applied to measuring nuclear morphology *in vitro* (7, 8). It has also been used to diagnose intraepithelial neoplasia (9) and to assess the efficacy of chemopreventive agents in an animal model of carcinogenesis (10). The latter study used the heterodyne a/LCI system used in this study to prospectively grade tissue samples based on the grading criteria developed in (9) without tissue processing. These studies showed that a/LCI can be used to assess neoplastic progression in an animal model of carcinogenesis. The high sensitivity and specificity achieved in these studies suggest the potential of the a/LCI technique as a noninvasive human diagnostic procedure.

The study presented here is a pilot study with the aim of establishing the ability of the a/LCI technique to assess neoplastic change in the respiratory tract of the Syrian golden hamster. The heterodyne a/LCI system offers an advantage over pathology in that it is a quantitative, near real-time, diagnostic instrument for detecting dysplasia by identifying nuclear morphology descriptors, such as changes in mean size and refractive index of the cell nuclei. Using the capability to measure these morphologic descriptors, the heterodyne a/LCI system was applied to the Syrian golden hamster model to

Received 5/23/06; revised 11/10/06; accepted 11/22/06.

Grant support: National Cancer Institute grants CN43308-13 and N01-CN-43308.

The costs of publication of this article were defrayed in part by the payment of page charges. This article must therefore be hereby marked *advertisement* in accordance with 18 U.S.C. Section 1734 solely to indicate this fact.

Requests for reprints: Adam Wax, Department of Biomedical Engineering, Box 90281, Duke University, Durham, NC 27708. Phone: 919-660-5143; Fax: 919-613-9144. E-mail: a.wax@duke.edu

doi:10.1158/1055-9965.EPI-06-0418

quantitatively distinguish between tracheal epithelial tissue that was classified by pathology as normal, low-grade dysplasia (LGD), and high-grade dysplasia (HGD). Although there were not enough samples used for this pilot study to confidently determine the statistical power of the approach, the results show clear separation and point to great promise in applying the a/LCI technique to the Syrian golden hamster model.

Materials and Methods

Chemicals. MNU was obtained from Ash Stevens, Inc. (Detroit, MI) and stored at −20°C.

Animals and Housing. All of the experimental protocols were in accordance with NIH guidelines and approved by the Institutional Animal Care and Use Committees of Duke University and The Ohio State University. Male Syrian golden hamsters 6 to 7 weeks of age were obtained from Charles River Laboratories (Wilmington, MA). Hamsters were kept in quarantine for 1 to 2 weeks before initiation of experimental procedures. Animals were housed in groups of three in plastic cages with hardwood bedding (Beta Chips, Northeastern Products Corp., Warrenburg, NY). Hamsters were fed the semipurified AIN-76A diet (Dyets, Bethlehem, PA), given water *ad libitum*, and maintained under standard conditions (20 ± 2°C, 50 ± 10% relative humidity, and 12-hour cycles of light and darkness). Hygienic conditions were maintained by twice-weekly changes of the animal cages.

Experimental Protocol. Carcinogen-treated animals were given MNU at a concentration of 0.5% once weekly for 10 weeks by intratracheal instillation, following (4). Ten weeks after completion of this dosing regimen, the animals were euthanized by CO_2 asphyxiation. Tracheas were excised and opened longitudinally for immediate spectroscopic analysis. After spectroscopic analysis, the tracheal samples were fixed in 10% neutral buffered formalin.

The experimental grouping of the eight samples is reported in Table 1. Each sample was interrogated at three points: 1 mm from the distal end, halfway between the distal and proximal ends, and 1 mm from the proximal end, adjacent to the larynx. The distal end was marked with India ink to aid in coregistration with histology.

Angle-Resolved Low-Coherence Interferometry. Intact *ex vivo* tissue samples were scanned using the heterodyne a/LCI technique (9, 10). The a/LCI technique uses coherence gating, made possible by the use of a low-coherence source (coherence length, ~30 μm), to probe tissue features at selected depths. The depth-resolved scattering distributions were obtained by the unique a/LCI imaging system that permits angular resolved scattering measurements. The a/LCI data, which is a function of scattering versus angle, were analyzed for a chosen depth in this study, specifically the epithelial layer. Identification of the epithelial layer for the a/LCI scan of hamster trachea is discussed below in Results. The a/LCI data acquired from biological tissue can be analyzed to obtain nuclear morphology descriptors, such as nuclear size and refractive index of the nucleus relative to the cytoplasm (n_{nuc}/n_{cyt}).

Table 1. Protocol for administration of NMU in the a/LCI study of Syrian golden hamster trachea

Group	No.	Treatment	Dose
1	3	Saline	N/A
2	3	MNU	0.5%
3	2	Control	N/A

The diameter of the probe beam is ~500 μm, meaning ~1,000 cells are interrogated at a given tissue layer simultaneously. This is advantageous because the instantaneous measurement of a scattering distribution from multiple cells within a region of interest provides an average that minimizes the effects of individual cellular variations in nuclear morphology. The scattering distribution consists of oscillations arising from the many constituents of the tissue. The scattering due to small scatterers and nuclear inhomogeneities is a slowly varying function of angle, which is removed from the spectrum by the subtraction of a second-order polynomial. Coherent scattering due to cell-to-cell correlations causes high-frequency oscillations, which are removed by using a low-pass filter (8, 11). After this processing, the measured scattering distribution due to the cell nuclei, which are present within the probe volume, is determined.

To statistically determine the relevant morphologic descriptors, the a/LCI data are compared with a database of theoretical predictions constructed using Mie theory (12). The theoretical scattering distributions are functions of several variables that define the scattering characteristics. These include the average scatterer diameter (d), which is varied between 5.0 and 20.0 μm in 0.1-μm increments, the refractive index of the scatterer relative to the surroundings (n_{scat}/n_{surr}), which is varied between 1.010 and 1.10 in 49 discrete steps, and the size distribution, which is based on a Gaussian distribution of sizes characterized by d and its SD (δd). The processed a/LCI data are compared with the database of similarly processed theoretical predictions, and the best fit is assessed using χ^2 minimization. Based on this fit, the morphologic descriptors of the cell nuclei, including average nuclear size and relative refractive index, within the region of interest are determined for each scanned point.

Histologic Grading of Neoplastic Tissues. Each fixed trachea sample was paraffin embedded with the epithelium uppermost. Longitudinal sections were cut (4 μm), mounted on a microscope slide, and stained with H&E. The locations of the sites scanned by the a/LCI system were identified by the location relative to the ink marking at the distal end. The region was then classified as normal epithelium, LGD, or HGD according to the microscopic descriptions of dysplasia given in Cotran et al. (13).

Statistical Analysis. For each histologic classification, the mean and SD from the mean of the a/LCI nuclear size measurements across samples was determined. Additionally, the mean and SD from the mean of the refractive index of the nucleus relative to the cytoplasm across samples were established. To assess the diagnostic capacity of the a/LCI method, doubled-sided t tests were done with the online software offered by Simple Interactive Statistical Analysis[4] to compare the a/LCI morphologic descriptors. The nuclear size and refractive index of the nucleus relative to the cytoplasm were compared between the classifications; the statistical difference was quantified by the P value obtained from the t test (reported below).

Additionally, a leave-one-out cross validation was done to calculate the sensitivity and specificity of the a/LCI technique. As discussed below, a separation between normal and diseased tissue was observed when the measurement was graphed as a function of refractive index and nuclear size. Based on that separation, each point was treated as a test point individually, whereas the remaining data were treated as a training set. A linear discriminant analysis (14) was done in Matlab (Mathworks), on the training set, and the test point was classified as diseased or normal based on its locus to the

[4] http://home.clara.net/sisa/t-thlp.htm

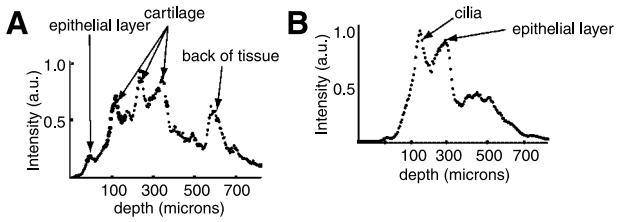

Figure 1. Depth scan integrated over angles for (**A**) tissue that does not present the mucous layer atop the ciliated epithelium. Three cartilage peaks and a peak that corresponds to the back of the tissue are observed. **B.** Tissue that presents a mucous layer atop the ciliated epithelium.

decision line. The predictions of the leave-one-out cross validation were compared with the histologic classification to calculate the sensitivity and specificity.

Results

Tissue Features. To orient our measurements to the tracheal epithelium, the a/LCI spectra were integrated across scattering angle to yield a depth-resolved reflection profile of the tissue. The profile was then compared with histologic slides to determine the location of the epithelium. In past a/LCI studies of rat esophagi (9, 10), the peak closest to the tissue surface was identified as the epithelium and used for analysis. The picture was not as immediately clear in the a/LCI data for the hamster tracheal tissues.

Two typical orientations from two different sampling sites are presented in the depth plots shown in Fig. 1. These two plots show the variability in tissue architecture that arose in the analysis of the hamster trachea tissue. The peak closest to the tissue surface can be attributed to one of two structures that were distinguished by the determined morphologic descriptors. In some cases, a small scatterer size with a large n_{scat}/n_{surr} was obtained for the topmost peak consistent with the size of cell nuclei observed in histopathologic slides, but in other cases, a larger scatterer size with a smaller n_{scat}/n_{surr} was obtained, which does not correspond to the observed cell nuclei morphology in the epithelium. We theorize that the second possibility arose due to a mucous layer atop the ciliated epithelium. In Fig. 1A, the mucous layer atop the ciliated epithelium is not present and the topmost peak is deemed the epithelial layer. In this profile, strong peaks due to the cartilage below the epithelial layer are seen, as well as a scattering peak due to the back of the tissue. In Fig. 1B, the topmost peak yielded a large scatterer size and a small n_{scat}/n_{surr} and is believed to arise from the mucous layer. In this case, the second topmost peak was determined to be the epithelial layer. In this sampling site, there is no cartilage present and thus no high-intensity backscattering peaks are observed in the profile. The differences in the scattering profiles depend on the theorized presence or absence of a mucous layer, which may have arisen due to slight differences in the way the tissues were handled between tissue harvest and spectroscopic analysis. We note that there is no obvious correlation between the presence of a mucous layer and the observation of the underlying cartilage. When further studies are done, the presence or absence of a mucous layer will be standardized by adapting more consistent tissue handling procedures.

Histologic Grading. Histologic analysis was done at all points scanned using a/LCI, provided that the site of measurement was identifiable. Some sites were not coregistered with histologic analysis due to processing artifacts or uncertainty of the measurement site and were thus omitted from the analysis. In group 1, there were three samples measured. Of those three samples, there were eight sampling sites available for histologic analysis, all of which were determined by histology to be normal. One site could not be coregistered with histology. In group 2, there were three samples measured. Of those three samples, there were nine sampling sites, all but two of which were determined to be LGD by histologic analysis. The other two sampling sites registered HGD. In group 3, there was two samples measured; only one was available for coregistration. Three sampling sites were measured on that sample, all of which were determined by histologic analysis to be normal tissue.

a/LCI Distributions. Typical measured a/LCI distributions for each pathologic tissue classification (normal epithelium, LGD, and HGD) are shown in Fig. 2. The a/LCI distribution is scattering as a function of angle, measured relative to the direct backscatter angle, for the depth corresponding to the epithelial layer. The data were processed, as described above; to extract the oscillatory component, which was then used to assess the morphologic variables through comparison to theoretically determined scattering distributions. The processed a/LCI distribution for each representative tissue classification is shown along with the corresponding best-fit theoretical distribution, which yields the size of the cell nuclei, within $\pm$ 0.3 μm, as well as n_{nuc}/n_{cyt}. H&E-stained micrographs of the tissue sections from the sites of the a/LCI measurements are also shown in Fig. 2.

The a/LCI-measured nuclear morphology measurements, along with the histologic classifications, are reported in

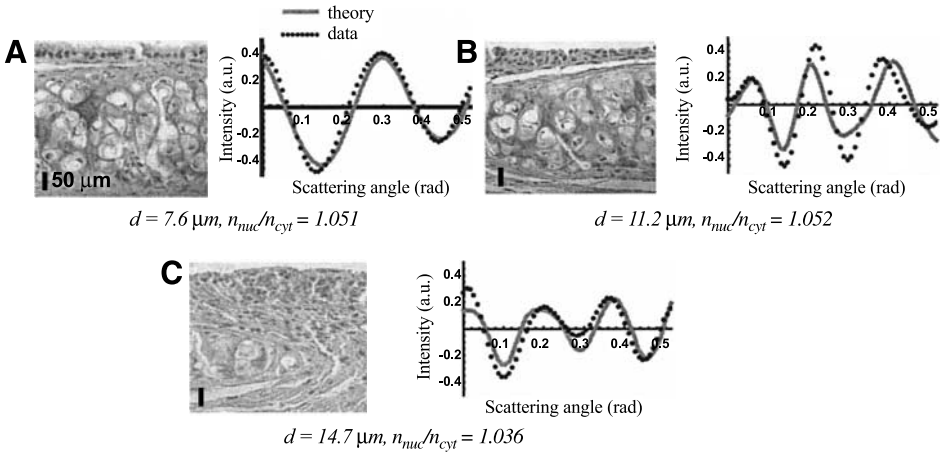

Figure 2. H&E-stained microscopy image (*left*, bar, 50 μm) and corresponding a/LCI ata, giving scattering as a function of angle, shown with best-fit theoretical distribution (*right*) for normal tissue (**A**), LGD (**B**), and HGD (**C**). The a/LCI determined nuclear morphology descriptor for each representative tissue type is given under each plot.

Table 2. Histologic classification versus the morphologic measurements determined by the a/LCI technique with the *P* values that signify the statistical significance of the difference between normal tissue/LGD and normal tissue/dysplastic tissue for (a) nuclear size and (b) n_{nuc}/n_{cyt}.

	Histologic classification			
	Normal	LGD	HGD	Dysplastic
Number	11	7	2	9
Size (μm)	7.00	10.1	15.2	11.2
σ (μm)	1.09	2.49	N/A	3.12

$P < 0.02$

$P < 0.01$

(a)

	Histologic classification			
	Normal	LGD	HGD	Dysplastic
Number	11	7	2	9
n_{nuc}/n_{cyt}	1.057	1.052	1.033	1.048
σ (μm)	0.006	0.010	N/A	0.010

(b)

Table 2 and shown graphically in Fig. 3. The data indicate an increase in nuclear size with increasing neoplastic progression. In tissues exposed to MNU, the average nuclear size in the scanned normal control tissues was found to be 7.00 ± 1.09 μm, where the error given here is the SD of the determined nuclear size across the samples. The nuclear size increased to 10.1 ± 2.49 μm for the tissues classified as LGD and 15.15 μm for the HGD tissues (there were too few HGD tissue samples to report a meaningful SD). A significant difference was found between the normal and LGD mean sizes ($P < 0.02$) and between normal and dysplastic (LGD + HGD) tissue ($P < 0.01$). Additionally, the measured n_{nuc}/n_{cyt} decreased with increasing neoplastic change (Fig. 3). The average n_{nuc}/n_{cyt} for normal tissues was 1.057 ± 0.006 and decreased to 1.052 ± 0.010 for LGD. The average n_{nuc}/n_{cyt} for dysplastic tissue (LGD + HGD) was found to be 1.048 ± 0.010, which is significantly different from that found for the normal tissues ($P < 0.05$). The trend toward decreasing n_{nuc}/n_{cyt} with increasing neoplastic change is an important new result.

Using both refractive index and nuclear size to characterize the data, diseased and normal tissue states can be separated (Fig. 3). Based on the results of the leave-one-out cross validation, the sensitivity is 78% (7/9) and the specificity is 91% (10/11). There was one false positive and two false negatives. The importance of these findings is discussed below.

Discussion

The present pilot study evaluated nuclear morphology in the Syrian golden hamster respiratory tract carcinogenesis model using the a/LCI technique. The first challenge to overcome in applying the heterodyne a/LCI system to this model was that of the tracheal geometry (i.e., the presence of a mucous layer atop the ciliated epithelium). This feature was not always observed, but the a/LCI technique was able to discriminate between scattering due to cilia within the mucous layer and that typical of cell nuclei by the differences in size and refractive index obtained from the analysis. These descriptors provided a way to differentiate the mucous layer from the epithelium in the a/LCI measurements. On identifying the presence of the mucous layer, the nuclear morphology of the epithelium was extracted from the next deepest layer, which is the epithelial layer.

Mean nuclear size has been established as a powerful indicator of neoplastic progression, with nuclear size increasing with escalating degrees of dysplasia (13). The a/LCI technique is a useful tool for detecting neoplastic progression in the epithelial layer through nuclear size measurements (9, 10). Using the heterodyne a/LCI system, normal and dysplastic tissues were distinguished in this pilot study. It was also observed in this study that the refractive index of the cell nucleus relative to the cytoplasm decreased as the degree of dysplasia increased. This nuclear morphology descriptor also enabled normal tissue to be distinguished from LGD, as well as from dysplastic tissue (LGD + HGD). The refractive index of the cell nucleus relative to the cytoplasm is a promising emerging biomarker, and, along with the nuclear size, will be an important measure of nuclear morphology in future studies.

In this study, the a/LCI technique distinguished normal from diseased tissue with a sensitivity of 78% (7 of 9) and a specificity of 91% (10 of 11). These sensitivity and specificity figures were obtained using both nuclear size and refractive index of the cell nucleus relative to the cytoplasm. The relatively low number of samples used in the study is a weakness in determining the discriminatory power of the technique. However, the results we present should be viewed as a pilot study, intended to determine the feasibility of the approach. Based on the results of leave-one-out cross-validation, used to calculate the sensitivity and specificity, the technique seems to be sufficiently accurate to warrant a more extensive study. Another potential concern with this application of a/LCI for the purpose is the reproducibility of the measurements. Although the small sample size used in this study cannot address this concern, we have studied previously the reproducibility of a/LCI measurements in an animal carcinogenesis model (9, 10). In these previous studies, we observed variation in mean nuclear size based on the age of the animal and dosing regimen. These trends could not be adequately identified in the current pilot study due to the insufficient number of samples. In the planned future study, we will analyze the nuclear morphology data to assess these trends and include them in establishing diagnostic criteria.

The heterodyne a/LCI system has shown the potential to become a valuable diagnostic tool for assessing nuclear

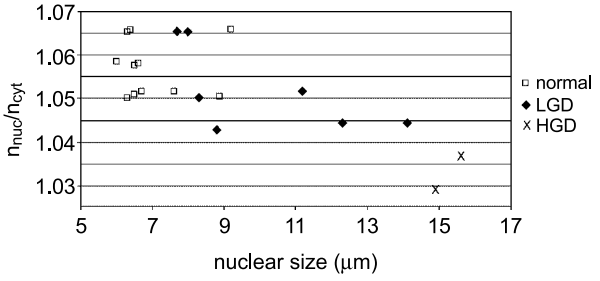

Figure 3. Histologic classification versus average cell nuclei size and average refractive index of the nucleus relative to the cytoplasm as determined by the a/LCI technique.

morphology in the hamster trachea model of carcinogenesis. The a/LCI nuclear morphology measurements can distinguish the epithelial layer from other features of the hamster trachea tissue, such as the mucous layer and cartilage. The measured nuclear morphology can be used to create two biomarkers of neoplastic change in the epithelial layers, the mean nuclear size and the refractive index of the nucleus relative to the cytoplasm. Using the a/LCI technique to evaluate tissue health enables detection of cancer progression and facilitates evaluation of prospective chemopreventive agents in parallel with assessing molecular alterations in the Syrian golden hamster respiratory model. The a/LCI technique is presently limited to visualizing preclinical cancer of the large airways, the origin of only a minority of human lung cancers. However, this new tool, once fully developed, may someday form the basis for a noninvasive fiber optical procedure to assess intraepithelial neoplasia in human bronchus to diagnose and assess risk of lung cancer. Furthermore, differences in optical light scattering could be used as a surrogate intermediate biomarker in phase II clinical trials to determine the efficacy of candidate agents to prevent lung cancer.

References

1. Ries LAG, et al. SEER Cancer Statistics Review, 1975–2002. Bethesda (MD): National Cancer Institute; 2005.
2. Travis WD, Sobin LH. Histological typing of lung and pleural tumours. Berlin, New York: Springer; 1999.
3. Moon RC, Rao KV, Detrisac CJ, Kelloff GJ. Hamster lung cancer model of carcinogenesis and chemoprevention. Adv Exp Med Biol 1992;320:55–61.
4. Grubbs CJ, Becci PJ, Thompson HJ, Moon RC. Carcinogenicity of *N*-methyl-*N*-nitrosourea and *N*-ethyl-*N*-nitrosourea when applied to a localized area of the hamster trachea. J Natl Cancer Inst 1981;66:961–5.
5. Huang D, Swanson EA, Lin CP, et al. Optical coherence tomography. Science 1991;254:1178–81.
6. Izatt JA, Kulkarni MD, Wang HW, Kobayashi K, Sivak MV. Optical coherence tomography and microscopy in gastrointestinal tissues. IEEE Journal of Selected Topics in Quantum Electronics 1996;2:1017–28.
7. Wax A, Yang CH, Backman V, et al. Cellular organization and substructure measured using angle-resolved low-coherence interferometry. Biophys J 2002;82:2256–64.
8. Pyhtila JW, Ma H, Simnick AJ, Chilkoti A, Wax A. Determining long range correlations by observing coherent light scattering from *in vitro* cell arrays with angle-resolved low coherence interferometry. J Biomed Opt 2006;11:024603.
9. Wax A, Yang CH, Muller MG, et al. *In situ* detection of neoplastic transformation and chemopreventive effects in rat esophagus epithelium using angle-resolved low-coherence interferometry. Cancer Res 2003;63:3556–9.
10. Wax A, Pyhtila JW, Graf RN, et al. Prospective grading of neoplastic change in rat esophagus epithelium using angle-resolved low-coherence interferometry. J Biomed Opt 2005;10:051604.
11. Pyhtila JW, Graf RN, Wax A. Determining nuclear morphology using an improved angle-resolved low coherence interferometry system. Optics Express 2003;11:3473–84.
12. van de Hulst HC. Light scattering by small particles. Structure of matter series. New York: Wiley; 1957.
13. Cotran RS, Robbins SL, Kumar V. Robbins pathologic basis of disease. Philadelphia: Saunders; 1994.
14. Webb AR; NetLibrary Inc. Statistical pattern recognition. West Sussex, England, New Jersey: Wiley; 2002. p. 496, xviii.